Instantaneous Current and Average Power Flow Characterization of a DC-DC-DC Triple Active Bridge Converter

Jonathan Saelens, Lauryn Morris, Oroghene Oboreh-Snapps, Arnold Fernandes, Praneeth Uddarraju, Sophia A. Strathman, and Jonathan W. Kimball
Department of Electrical and Computer Engineering - Missouri University of Science and Technology
{jhskrw@mst.edu, lrmdhf@mst.edu, oogdq@mst.edu, af2vc@mst.edu, pu5mb@mst.edu, ss6k4@mst.edu, kimballjw@mst.edu}

2024 IEEE Power and Energy Conference at Illinois (PECI) | 979-8-3503-7220-5/24/$31.00 ©2024 IEEE | DOI: 10.1109/PECI61370.2024.10525254

***Abstract*—The Triple Active Bridge (TAB) is a three-port power converter that facilitates bi-directional power flow and provides galvanic isolation, making it a subject of significant research attention. This is attributed to its diverse applications in high-frequency DC-DC conversion, electric vehicles, renewable energy integration, and micro-grids. Controlling the system at run-time involves modification of the two phase-shift parameters between respective bridges. By analyzing the fundamental converter operating equations, future control designers can use this framework to optimize control schemes to mitigate the under-determined nature of the TAB converter. In this paper, we elucidate the foundational operational principles of the TAB and establish the defining equations for instantaneous current and average power flow. Furthermore, we validate these equations through a comparative analysis involving a simulation model of the TAB in PLECS and hardware implementation.**

***Index Terms*—Triple Active Bridge, DC-DC Converter, Bi-directional, Power Electronics, Instantaneous Current, Average Power, High Frequency Conversion.**

I. Introduction

THE dual active bridge (DAB), a classification of solid-state transformers [1], is a dual H-bridge power converter renowned for its many admirable qualities, including bi-directional power flow capability, high conversion efficiency, galvanic isolation, and low component counts [2], [3]. Its well-understood topology and varied control strategies make it a exceptional and robust candidate for many of today's high-power applications such as electric vehicle chargers and micro-grids [4]. Although the DAB is currently widely used, it's important to note that the single-source single-sink configuration is not sufficient for all use cases. The triple active bridge (TAB), on the other hand, still retains all of these beneficial qualities while improving on the DAB's core structure [5]. Through the inclusion of a third bridge, the TAB allows for either single-source multi-sink or multi-source single-sink, offering adaptability depending on the desired implementation strategy. This enables the TAB to be used in many additional scenarios including modern onboard vehicle chargers, smart grids, and battery storage grid integration [6], [7].

Appropriately controlling the TAB converter requires understanding and analysis of the system's instantaneous current and average power by utilizing their respective equations. The main contribution of this paper is to present these defining TAB system equations, for use in future control schemes, while expanding on existing work presented in [8] and [9]. In Section II, a brief description of the TAB topology is provided. The proposed equations are then presented with a functional description of their derivation process in Section III. To verify efficacy, the equations are then compared against simulation and hardware in Section IV before concluding the paper and presenting a direction for future work in Section V.

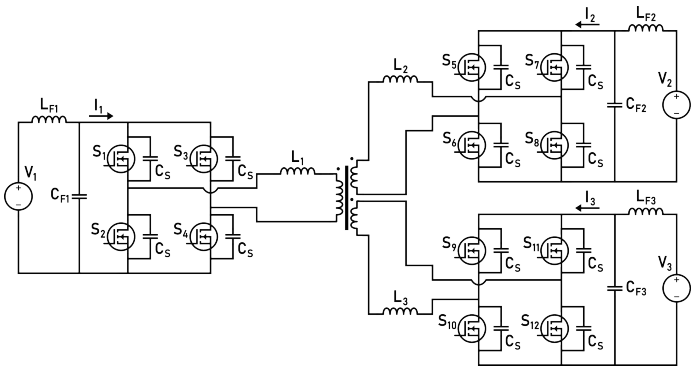

Figure 1: Topology of a DC-DC-DC triple active bridge power converter.

II. DC-DC-DC TAB Converter Topology

The triple active bridge converter is a three-bridge system that allows bi-directional power flow on each port and galvanic isolation between all ports. The diagram of the topology is available in Fig. 1. The TAB consists of three H-bridges connected through a high-frequency three-winding transformer [10]. Each bridge has a leakage inductance L_1, L_2, and L_3, typically incorporated within the transformer itself, that can be tuned to designate the amount of power transfer present throughout the system. In [11], a methodology for determining such inductances and the required transformer turns ratio is presented. The main control parameters, while the TAB is in operation, are the respective phase shift values between bridges, ϕ_2 and ϕ_3. Bridge 1 is designated as the reference bridge and has a phase shift of zero degrees. By modulating these two phase shift parameters, the amount of power transferred between bridges can be calculated as described in Section III. Further descriptions of the system will be discussed in the proceeding sections.

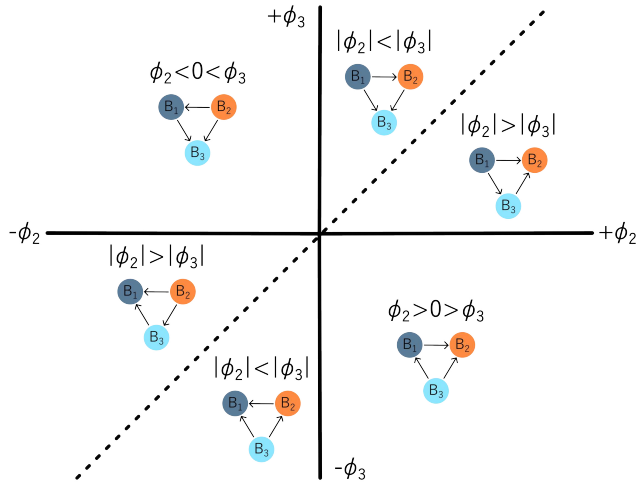

Figure 2: Diagram of six possible phase shift configurations within the TAB and their respective power transfer directions.

III. System Equations

Based on the typical TAB transformer design, the leakage inductance is significantly smaller than the internal magnetizing inductance. To simplify calculations, we can therefore assume that the magnetizing inductance, L_m, is infinite and hence may be ignored. The leakage inductor current is governed by:

$$I(\theta) = \frac{1}{L}\int_0^{\theta} V(\tau)\,d\tau + I(0) \tag{1}$$

To accurately incorporate the transformer turns ratios into the newly proposed equations, illustrating the relationship of translating voltages and inductances between two arbitrary windings, a and b, is necessary. These dependencies are exemplified by:

$$V_a = V_b\frac{N_a}{N_b} \tag{2}$$

$$L_a = L_b\left(\frac{N_a}{N_b}\right)^2 \tag{3}$$

The computation of average power, including a simplified version enabling current waveform analysis, is emphasized by:

$$P = \frac{1}{T}\int_0^{T} (V(t)\cdot I(t))\,dt \tag{4}$$

$$P = \frac{2V}{T}(A_1 + A_2 + A_3) \tag{5}$$

The incorporation of transformer turns ratios within the average power flow equations allows for more diverse usage scenarios. These ratios, $\frac{N_1}{N_2}$ and $\frac{N_1}{N_3}$, are denoted by n_{12} and n_{13}, respectively. The power flow on each port is given by:

$$P_1 = \frac{V_1V_2\phi_2L_3n_{12}n_{13}^2(\pi-|\phi_2|)}{2f_s\pi^2(L_1L_2n_{12}^2+L_1L_3n_{13}^2+L_2L_3n_{12}^2n_{13}^2)} + \frac{V_1V_3\phi_3L_2n_{12}^2n_{13}(\pi-|\phi_3|)}{2f_s\pi^2(L_1L_2n_{12}^2+L_1L_3n_{13}^2+L_2L_3n_{12}^2n_{13}^2)} \tag{6}$$

$$P_2 = \frac{V_2V_1\phi_2L_3n_{12}n_{13}^2(|\phi_2|-\pi)}{2f_s\pi^2(L_1L_2n_{12}^2+L_1L_3n_{13}^2+L_2L_3n_{12}^2n_{13}^2)} + \frac{V_2V_3L_1n_{12}n_{13}(\phi_2-\phi_3)(|\phi_2-\phi_3|-\pi)}{2f_s\pi^2(L_1L_2n_{12}^2+L_1L_3n_{13}^2+L_2L_3n_{12}^2n_{13}^2)} \tag{7}$$

$$P_3 = \frac{V_3V_1\phi_3L_2n_{12}^2n_{13}(|\phi_3|-\pi)}{2f_s\pi^2(L_1L_2n_{12}^2+L_1L_3n_{13}^2+L_2L_3n_{12}^2n_{13}^2)} + \frac{V_3V_2L_1n_{12}n_{13}(\phi_2-\phi_3)(\pi-|\phi_2-\phi_3|)}{2f_s\pi^2(L_1L_2n_{12}^2+L_1L_3n_{13}^2+L_2L_3n_{12}^2n_{13}^2)} \tag{8}$$

Instantaneous current for each of the six available phase shift combinations present within the TAB is governed by:

$$I_1 = \frac{A(L_2(V_1Bn_{12}^2+Hn_{12}^2n_{13})+L_3(V_1Bn_{13}^2+Gn_{12}n_{13}^2))}{4\pi f_s(L_1L_2n_{12}^2+L_1L_3n_{13}^2+L_2L_3n_{12}^2n_{13}^2)} \tag{9}$$

$$I_2 = \frac{-A(L_1(Gn_{12}^2-Hn_{12}n_{13})+L_3(V_1Bn_{12}n_{13}^2+Gn_{12}^2n_{13}^2))}{4\pi f_s(L_1L_2n_{12}^2+L_1L_3n_{13}^2+L_2L_3n_{12}^2n_{13}^2)} \tag{10}$$

$$I_3 = \frac{-A(L_1(Hn_{13}^2-Gn_{12}n_{13})+L_2(V_1Bn_{12}^2n_{13}+Hn_{12}^2n_{13}^2))}{4\pi f_s(L_1L_2n_{12}^2+L_1L_3n_{13}^2+L_2L_3n_{12}^2n_{13}^2)} \tag{11}$$

Where:

$$\theta = 2\pi\cdot\frac{\mathrm{mod}(t,T)}{T} \tag{12}$$

$$A = \mathrm{sgn}(\pi-\theta) \tag{13}$$

$$B = 2\theta + \pi(\mathrm{sgn}(\pi-\theta)-2) \tag{14}$$

$$C = A\cdot\mathrm{sgn}(|\phi_2|-\theta)\cdot\mathrm{sgn}(|\phi_2|+\pi-\theta) \tag{15}$$

$$D = A\cdot\mathrm{sgn}(|\phi_3|-\theta)\cdot\mathrm{sgn}(|\phi_3|+\pi-\theta) \tag{16}$$

$$E = A\cdot\mathrm{sgn}(|\phi_2|-\pi+\theta)\cdot\mathrm{sgn}(|\phi_2|-2\pi+\theta) \tag{17}$$

$$F = A\cdot\mathrm{sgn}(|\phi_3|-\pi+\theta)\cdot\mathrm{sgn}(|\phi_3|-2\pi+\theta) \tag{18}$$

$$G = \begin{cases} V_2(\pi + C(B+\pi-2|\phi_2|)) & \phi_2 \geq 0 \\ -V_2E(2(|\phi_2|+\theta)+\pi(A+E-3)) & \phi_2 < 0 \end{cases} \tag{19}$$

$$H = \begin{cases} V_3(\pi + D(B+\pi-2|\phi_3|)) & \phi_3 \geq 0 \\ -V_3F(2(|\phi_3|+\theta)+\pi(A+F-3)) & \phi_3 < 0 \end{cases} \tag{20}$$

IV. Results

To delineate the background of the newly proposed equations for instantaneous current and average power flow, this section provides a brief description of the method by which these equations were obtained and provides experimental data to further demonstrate their validity.

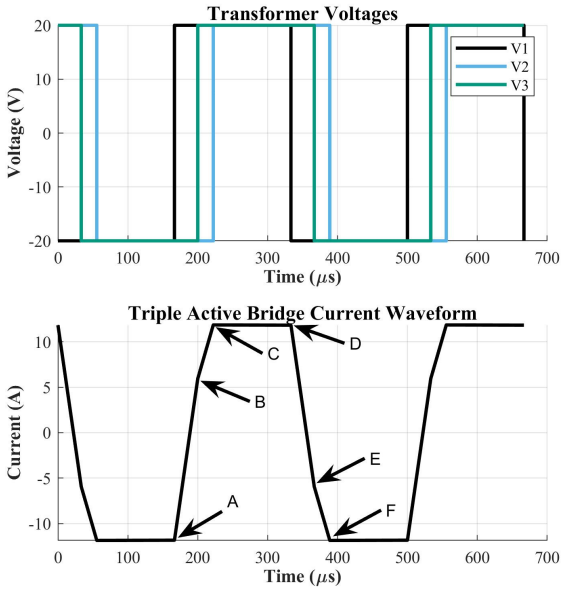

Figure 3: Periodic triple active bridge waveforms. Three-bridge transformer voltages and single-bridge (bridge 1) transformer current.

Switching Frequency	30 kHz
Duty Cycle	50%
Leakage Inductance L_1	12.26μH
Leakage Inductance L_2	7.186μH
Leakage Inductance L_3	18.34μH

Table I: Default TAB system parameters.

Turns Ratio (N_1:N_2:N_3)	1:1:1
Primary Voltage (V_1)	20V
Secondary Voltage (V_2)	20V
Tertiary Voltage (V_3)	20V

Table II: Unity transformer TAB system parameters.

Turns Ratio (N_1:N_2:N_3)	1:4:2
Primary Voltage (V_1)	20V
Secondary Voltage (V_2)	80V
Tertiary Voltage (V_3)	40V

Table III: Non-unity transformer TAB system parameters.

A. Instantaneous Current Equations

The under-determined nature of the TAB produces numerous valid solution combinations of ϕ_2 and ϕ_3. Analyzing the instantaneous current facilitates identifying a single configuration providing higher efficiency or improved converter response. The following analysis will utilize a positive current indicating power flow from the DC port toward the transformer, and a negative current indicating power flow from the transformer toward the DC port. The current waveform of the TAB contains six main segments, referenced in Fig. 3, where the current at point A is equal to the negative of the current at point D. Using the inductor current in (1), the instantaneous current at each of these six segments can be defined. In this equation, L is the inductance, V is the inductor voltage, and $I(0)$ is the initial current at $\theta = 0$.

By generating this equation for the first three linear time segments (A→B, B→C, and C→D) and performing substitu-

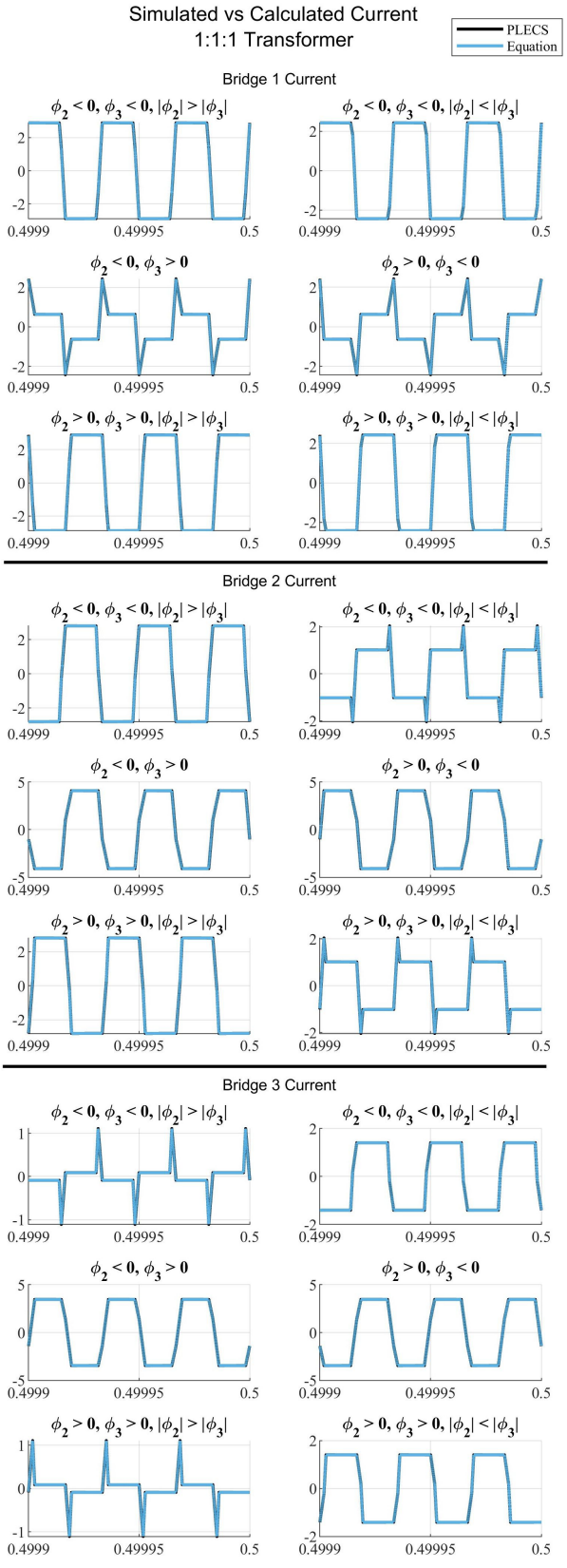

Figure 4: PLECS simulated system current vs calculated equation current with a 1:1:1 transformer ratio. The x-axis corresponds to time in seconds and the y-axis corresponds to current in amps. $T = \frac{1}{30{,}000}$.

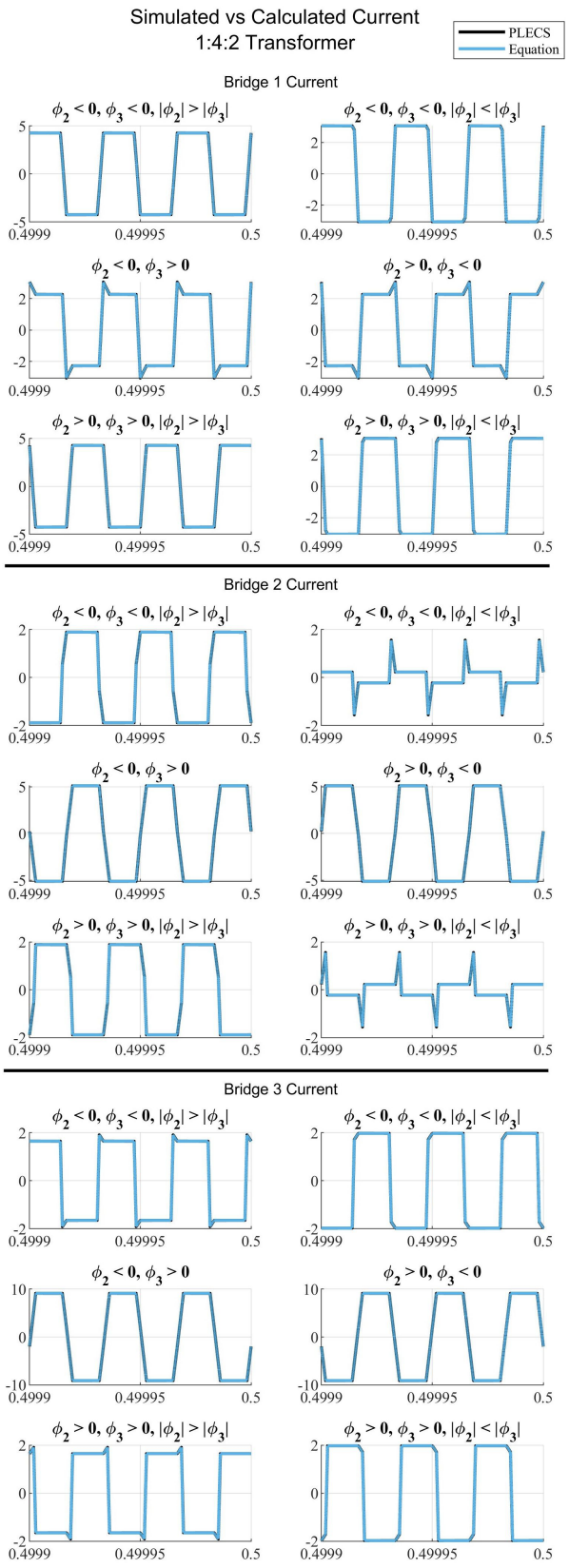

Figure 5: PLECS simulated system current vs calculated equation current with a 1:4:2 transformer ratio. The x-axis corresponds to time in seconds and the y-axis corresponds to current in amps. $T = \frac{1}{30{,}000}$.

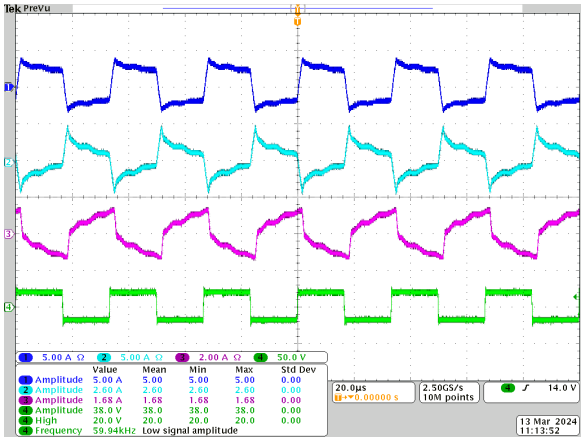

Figure 6: Instantaneous current TAB waveforms. Top to bottom: dark blue = bridge 1 current, light blue = bridge 2 current, pink = bridge 3 current, green = bridge 1 transformer voltage. $\phi_2 = 20°$, $\phi_3 = 30°$.

tion so each is dependent on I(A), the first equation evaluated at $\theta = A$ can be equated to the negative of the third equation evaluated at $\theta = D$ and solved for I(A), then substituted back into the original three equations. Repeating this for all phase combinations and bridges yields a multitude of equations, and performing algebraic manipulation, the resulting relationships are available in (9), (10), and (11).

1) Unity Transformer Case: For many applications within power electronics, a unity, or 1:1:1 turns ratio transformer is used. This allows for safety and noise isolation while not affecting output voltage. For this analysis, general system parameters are defined in Table I, and the transformer specifications are defined in Table II. Collecting data for three switching cycles before t = 0.5s to discount startup transients, Fig. 4 demonstrates that the PLECS simulations and the computed current equations line up identically thus validating the current equations for all phase combinations in Fig. 2.

2) Non-Unity Transformer Case: In many realistic applications, the same voltage magnitude on all bridges may not be desired. Because the duty cycle is not being modulated, the transformer turns ratio impacts the voltages. To incorporate the transformer turns ratios into the instantaneous current equations, voltages and inductances must be translated across a three-winding transformer. From the b winding to the a winding, the transfer is exemplified by (2) and (3), respectively. By including (2) and (3), it is possible to characterize the instantaneous current using any set of transformer turns ratios.

Utilizing the constant system parameters outlined in Table I and the non-unity transformer specifications defined in Table III, Fig. 5 illustrates that the simulated PLECS current and calculated equation current line up analogously.

3) Hardware Verification: The hardware setup consists of system elements defined in Table I and Table II. A photo of the complete setup is shown in Fig. 8. Because physical hardware incorporates non-idealistic elements that are not easily modeled through circuit simulation, it is expected to encounter slight deviations or signal ringing within the current waveforms. When comparing the graph presented in Fig. 6 to the waveforms for $\phi_2 > 0,\ \phi_3 > 0,\ |\phi_2| < |\phi_3|$ in Fig. 4, it can be seen that both possess similarities in waveform shape.

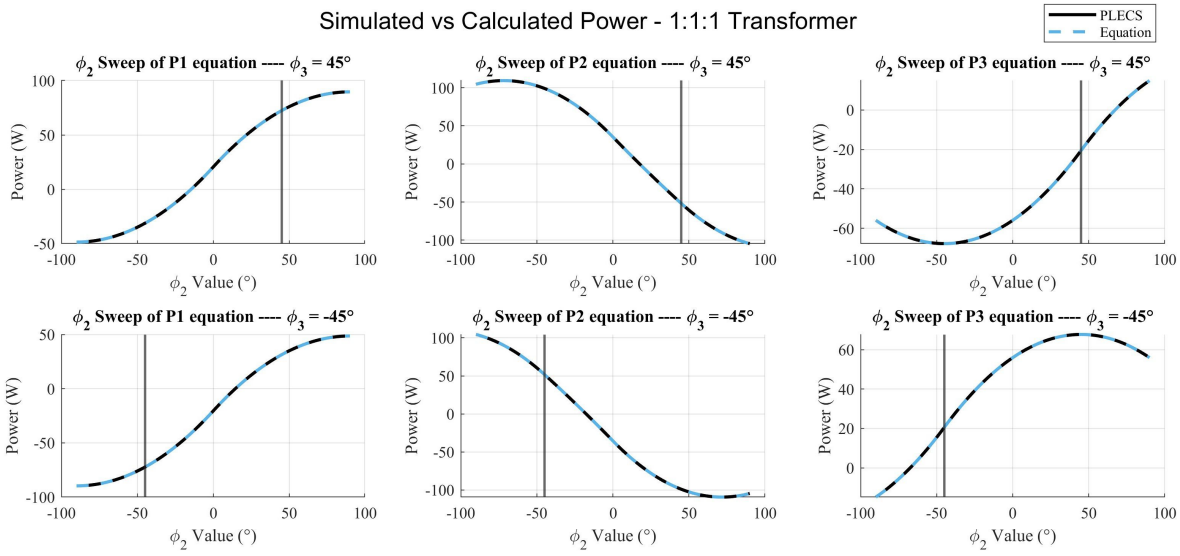

Figure 7: Sweep of ϕ_2 parameter comparing PLECS simulated power vs calculated equation power with varying ϕ_3 values for a 1:1:1 transformer ratio.

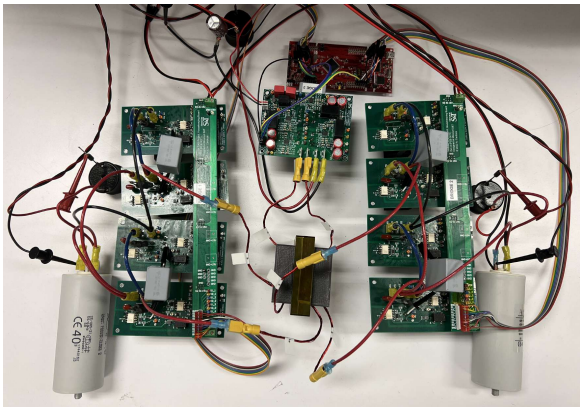

Figure 8: DC-DC-DC TAB hardware test setup.

B. Power Flow Equations

In a TAB, the power flowing through the system is characterized by the amount of power at one specific bridge, where a positive value indicates a power source and a negative value indicates a power sink. Based on the system configuration, the only atributes that can be modified while the converter is in operation are the phase shift parameters, ϕ_2 and ϕ_3. By using the quantity of desired power, the average power flow equations can be used to determine a possible configuration for ϕ_2 and ϕ_3 to meet demands.

Using P_1 as an example, the average power between P_1 and P_2 and then P_1 and P_3 are calculated using the general average power equation provided in (4) and then added versus analyzing the power due to all three bridges simultaneously. Since the power transfer in the first half of the switching cycle is equal to that in the second half, we can compute the average power by multiplying the integral of the first three time segments (from point A to point D) by the voltage and dividing by the time period, as in (5). Repeating this process for each of the bridges and phase combinations will yield a comprehensive list of defining equations. After further simplification and combination, these equations have been reduced and are indicated in (6), (7), and (8).

In an ideal system, the efficiency of any converter is equal to 100%. As an initial equation verification step, it is important to note that due to the conservation of power, computing the sum of P_1, P_2, and P_3, should result in a net value of zero. Summing (6), (7), and (8) yields this expected result.

1) Unity Transformer Case: To perform analysis on the average power equations, a parameter sweep for ϕ_2 was used rather than a time-dependent signal shown in the instantaneous current case. Utilizing the same system parameters, the graphs in Fig. 7 illustrate a sweep of ϕ_2 while keeping ϕ_3, the vertical line, constant. For all measured values of ϕ_2, the resulting equations exactly match the PLECS simulation outputs.

2) Non-Unity Transformer Case: When considering the non-unity transformer case, it is imperative that the power flow equations continue to hold to enable calculation of the phase shift parameters, ϕ_2 and ϕ_3. Using PLECS to measure simulated average system power and plotting these values against the newly proposed average power flow equations, the results, employing the same non-unity system parameters as before, can be seen in Fig. 9. All of the simulated PLECS waveforms precisely match the equations.

3) Comparison to Previous Work: In a typical triple active bridge application, following [8], bridge 1 is usually considered the primary source, with power also flowing from bridge 3 to bridge 2. This is dictated by positive phase shift values for both ϕ_2 and ϕ_3, and ϕ_2 being greater than ϕ_3. While scenarios where bridge 1 is a source and bridge 3 is either a source or sink are explored in [9], such cases limit the bi-directional capabilities of the TAB. To address this limitation, the newly proposed equations, accommodating all six modes of operation presented in Fig. 2, extend beyond the scope of previous studies. Unlike equations in [8], the updated mathematical formulations in (6), (7), and (8) incorporate transformer turn ratios, crucial for a comprehensive analysis.

Fig. 10, with a unity transformer, illustrates that the previous

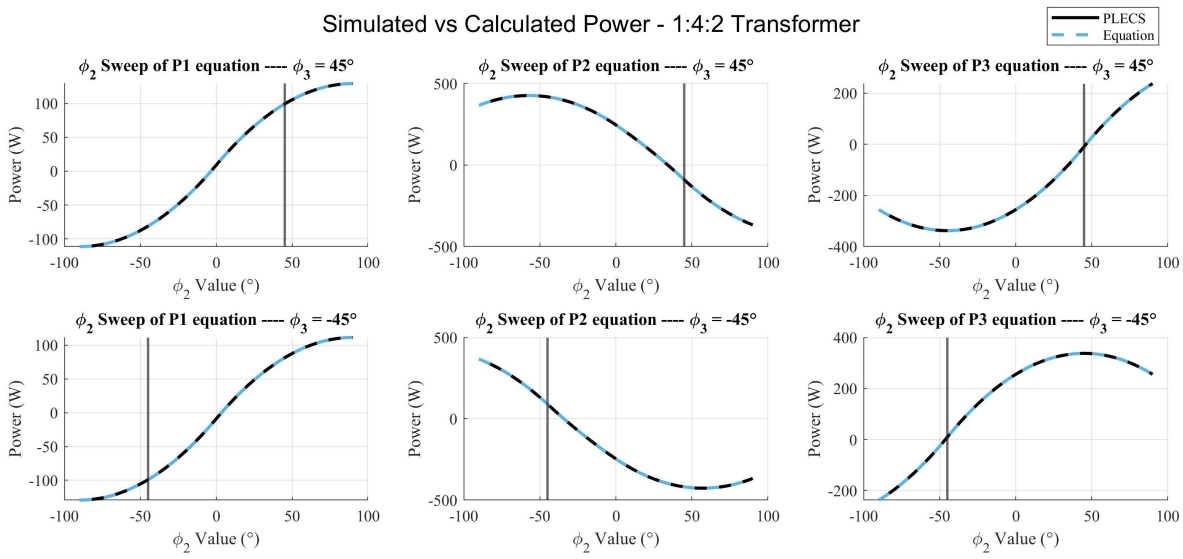

Figure 9: Sweep of ϕ_2 parameter comparing PLECS simulated power vs calculated equation power with varying ϕ_3 values for a 1:4:2 transformer ratio.

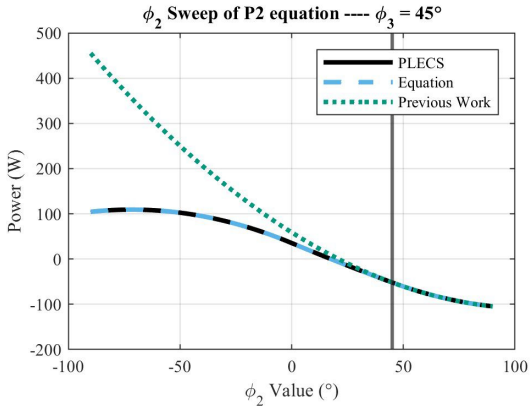

Figure 10: Comparison of P_2 equation of PLECS output vs newly proposed equations vs previous work.

equations from [8] hold true only when $\phi_2 > \phi_3$. Conversely, the introduced equations consistently match PLECS results across the entire range of ϕ_2 values, irrespective of ϕ_3. Employing different transformer turn ratios reveals a stark divergence, where the previous equations deviate significantly from the simulated PLECS curve, while the presented mathematical expressions maintain their expected behavior.

V. Conclusion

The triple active bridge is a sophisticated power converter containing a wide array of system variables. Through the examination provided above, a set of defining equations for both instantaneous current and average power have been presented which encompass all possibilities of transformer turns ratios and phase configurations. Their efficacy has been validated through analysis of PLECS simulations and hardware implementation. Presenting a direction for future work includes developing an appropriate control strategy for effectively calculating phase shift parameters ϕ_2 and ϕ_3. In addition, adaptation of the presented equations to allow for one or more bridges to interface with AC rather than solely DC would allow for more diverse converter applications.

References

[1] Xu She, Alex Q. Huang, and Rolando Burgos. Review of solid-state transformer technologies and their application in power distribution systems. *IEEE Journal of Emerging and Selected Topics in Power Electronics*, 1(3):186–198, 2013.

[2] Hengsi Qin and Jonathan W. Kimball. Solid-state transformer architecture using ac–ac dual-active-bridge converter. *IEEE Transactions on Industrial Electronics*, 60(9):3720–3730, 2013.

[3] Kartikeya Jp Veeramraju, Angshuman Sharma, and Jonathan W. Kimball. A comprehensive analysis on complex power flow mechanism in an ac-ac dual active bridge. In *2022 IEEE Power and Energy Conference at Illinois (PECI)*, pages 1–6, 2022.

[4] Angshuman Sharma, Kartikeya Jp Veeramraju, and Jonathan W. Kimball. Power flow control of a single-stage ac-ac solid-state transformer for ac distribution system. In *2022 IEEE Power and Energy Conference at Illinois (PECI)*, pages 1–6, 2022.

[5] Subhradip Mukherjee and Indrajit Sarkar. A brief review on triple active bridge dc-dc converter. In *2023 IEEE International Students' Conference on Electrical, Electronics and Computer Science (SCEECS)*, pages 1–6, 2023.

[6] Shenli Zou, Jiangheng Lu, Ayan Mallik, and Alireza Khaligh. Modeling and optimization of an integrated transformer for electric vehicle onboard charger applications. *IEEE Transactions on Transportation Electrification*, 4(2):355–363, 2018.

[7] Viju Nair R., Srinivas Gulur, Ritwik Chattopadhyay, and Subhashish Bhattacharya. Integrating photovoltaics and battery energy storage to grid using triple active bridge and voltage source converters. In *IECON 2020 The 46th Annual Conference of the IEEE Industrial Electronics Society*, pages 3691–3696, 2020.

[8] Chuanhong Zhao, Simon D. Round, and Johann W. Kolar. An isolated three-port bidirectional dc-dc converter with decoupled power flow management. *IEEE Transactions on Power Electronics*, 23(5):2443–2453, 2008.

[9] Ritwik Chattopadhyay, Sayan Acharya, Ghanshyamsinh Gohil, and Subhashish Bhattacharya. One switching cycle current control strategy for triple active bridge phase-shifted dc-dc converter. In *2017 IEEE Industry Applications Society Annual Meeting*, pages 1–8, 2017.

[10] Babak Rahrovi, Ramin Tafazzoli Mehrjardi, and Mehrdad Ehsani. On the analysis and design of high-frequency transformers for dual and triple active bridge converters in more electric aircraft. In *2021 IEEE Texas Power and Energy Conference (TPEC)*, pages 1–6, 2021.

[11] Venkateswara Rao Kudaravalli, Vishwabandhu Uttam, and Vishnu Mahadeva Iyer. A design methodology for triple active bridge dc- dc converter. In *2022 IEEE International Conference on Power Electronics, Drives and Energy Systems (PEDES)*, pages 1–7, 2022.